

Effect of mechanical damage on thermal conduction of plasma-sprayed coatings

Lanhua Wei,^{a)} Antonia Pajares,^{b)} and Brian R. Lawn

Materials Science and Engineering Laboratory, National Institute of Standards and Technology, Gaithersburg, Maryland 20899

(Received 20 September 1995; accepted 29 February 1996)

A thermal wave methodology for monitoring the thermal conduction of ceramic coatings with accumulating mechanical damage is described. Tests are conducted on a model alumina coating containing laminar defect intralayers. Controlled subsurface damage introduced with a spherical indenter is observed using a presectioned specimen. Microcrack damage accumulates progressively with increasing contact load and number of cycles. Associated changes in thermal diffusivity, specifically in the through-thickness direction, are imaged and quantified point-by-point using laser-generated thermal waves. The effective thermal resistance of the coating increases with crack density, up to the point of failure.

Plasma-sprayed ceramics are used to provide protective coatings on metal substrates.¹⁻³ They are particularly useful as thermal barrier coatings, where thermal insulation is paramount to the survival of underlayer metal components.¹⁻⁴ However, such coatings tend to have a high defect content, and are susceptible to damage accumulation, particularly in cycling, and therefore have finite mechanical lifetimes. Accordingly, it can be important to understand how thermal properties change with damage evolution.

In the present study we use a thermal wave technique^{5,6} to investigate the effect of mechanical damage accumulation on the thermal properties of ceramic coating structures. The technique provides point-by-point information on the distribution of damage within the structures. Hertzian testing with a spherical indenter is used to introduce the damage in a simple but controlled way, and to follow the evolution of this damage as a function of contact load and number of cycles. The Hertzian test, with its highly concentrated stress field, is especially useful in probing weak points within the coating/substrate structure. Such testing has already been used in earlier studies to investigate damage accumulation in alumina-based ceramic coatings, as well as in other coating system.^{7,8} Although alumina is not a common component of practical thermal barrier coatings, we retain this material from those earlier studies as an ideal model system for demonstrating the thermal wave procedure.

Nominally pure alumina coatings were air plasma sprayed directly onto grit-blasted soft steel substrates ≈ 3 mm thick (i.e., without bond coat) to produce coating/substrate coupons.^{7,8} The coatings were deposited to a thickness ≈ 500 μm in four interrupted torch passes, leaving defective intralayer interfaces in the structure. Specimens with surface dimensions

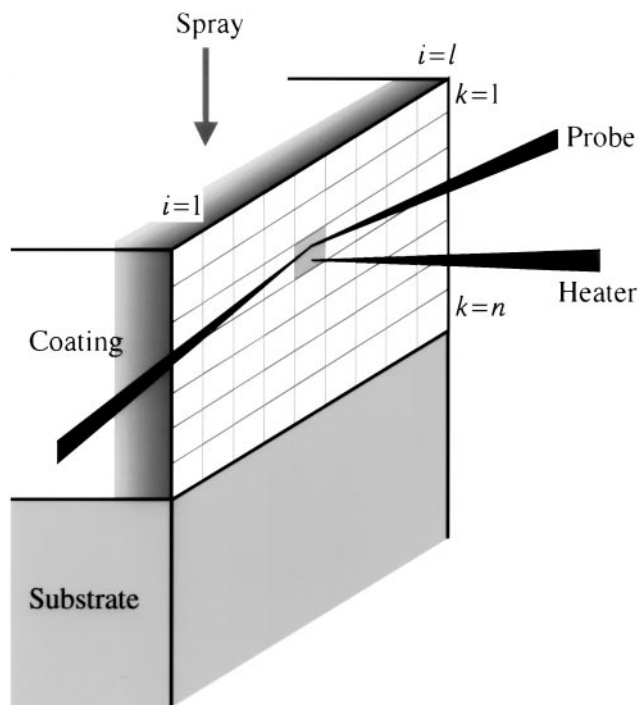


FIG. 1. Schematic of thermal wave imaging setup, showing heating and probe beam configuration over selected area of coating cross sectional area, subdivided into $l \times n$ array of pixels. Graded shade region behind image section area indicates diffusion depth of thermal waves. Arrow indicates spray direction onto coating surface.

^{a)}Guest Scientist, on leave from Department of Physics and Astronomy, Wayne State University, Detroit, Michigan.

^{b)}Guest Scientist, from Departamento de Física, Universidad de Extremadura, 06071 Badajoz, Spain.

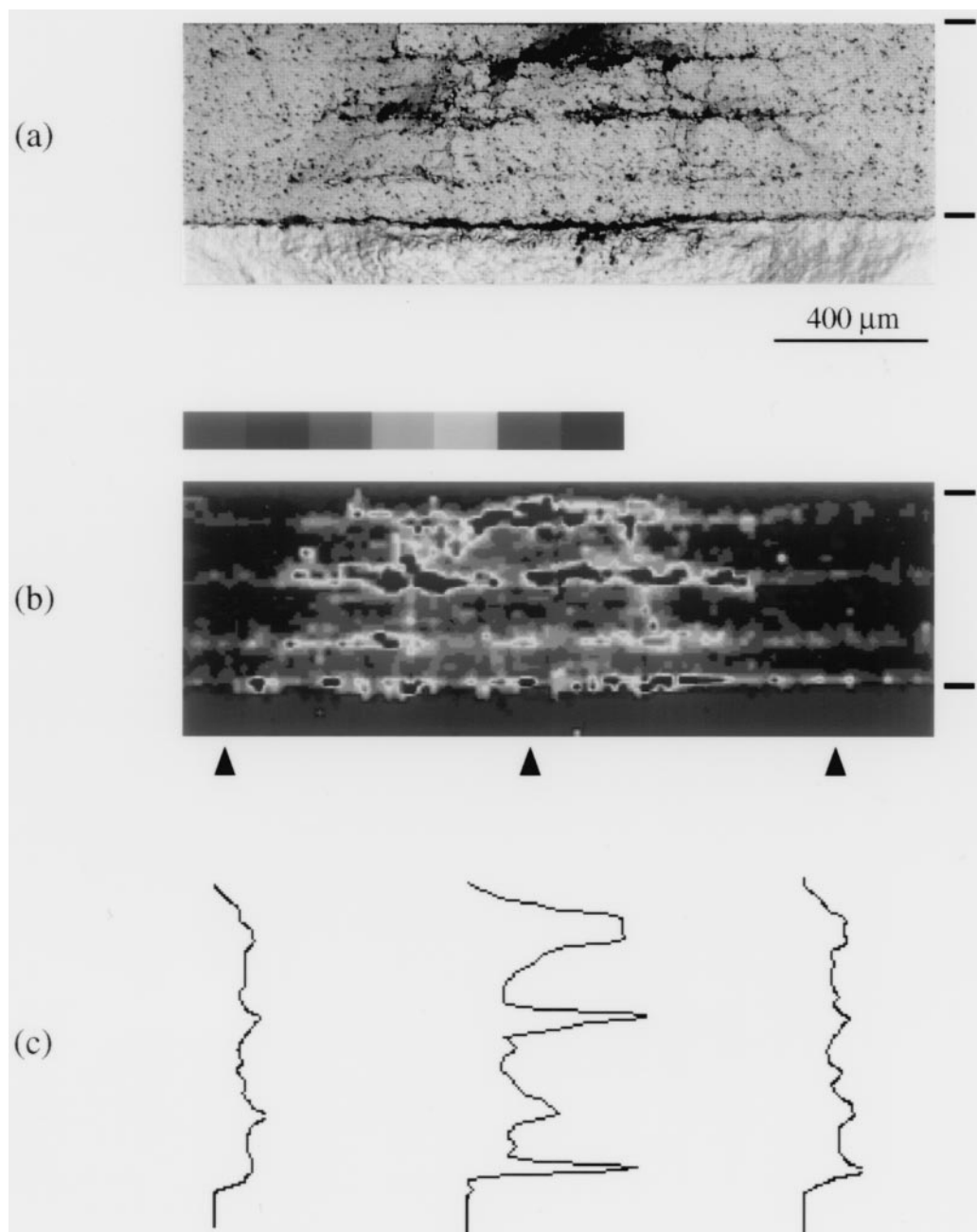


FIG. 2. Damage in alumina coating, thickness $\approx 500 \mu\text{m}$, on steel substrate. Load 1000 N, single cycle. (a) Optical micrograph, (b) thermal wave image, and (c) magnitude traces through thickness. Note damage along intracoating defect layers. Horizontal lines indicate coating top surface and coating/substrate interface. Vertical arrowheads indicate locations of magnitude traces. Color bar indicates signal magnitude, increasing temperature from blue to red end of scale. (Thermal wave conditions: frequency 500 Hz, raster step size $20 \mu\text{m}$, heating beam radius $4 \mu\text{m}$, probe beam radius $10 \mu\text{m}$, and heating/probe beam distance $10 \mu\text{m}$.)

$25 \times 3.5 \text{ mm}$ were then cut from the coupons. Cross sections from adjacent cuts were polished to $1 \mu\text{m}$ finish and screwed back together through carefully aligned holes in the metal substrates.⁷ The tops of the bonded specimens were then lightly ground and final polished to a $1 \mu\text{m}$ flat finish. Hertzian tests were made symmetrically on these top surfaces, along the traces of the bonded interfaces, using tungsten carbide

spheres of radius $r = 3.18 \text{ mm}$ at prescribed loads and at a cycle frequency of 10 Hz. After separation, the bar sections were cleaned and gold coated, then examined by Nomarski interference microscopy to reveal the subsurface damage.

The thermal wave technique is described elsewhere.^{5,6} For the present work, the specific configuration shown schematically in Fig. 1 is used. The specimen

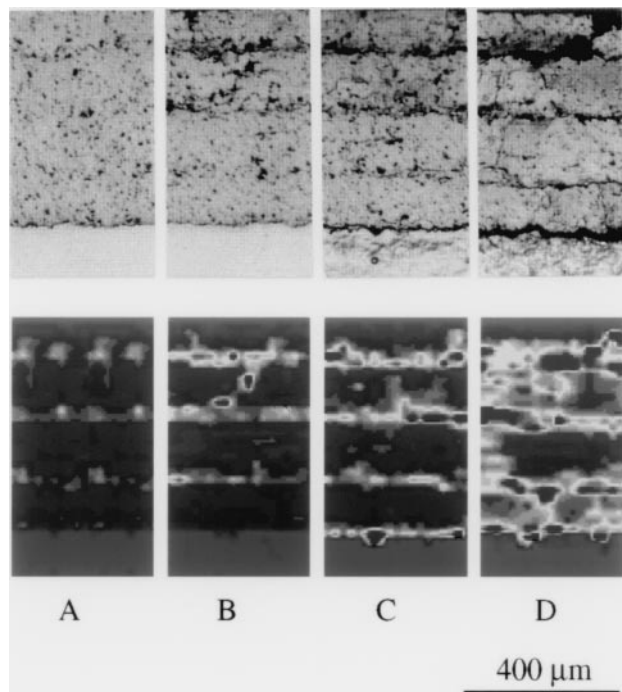


FIG. 3. Optical micrographs (top) and thermal wave images (bottom) of damage areas in alumina coating immediately below contact surface, for peak loads (A) 0, (B) 150 N, (C) 500 N, and (D) 1500 N, over a single cycle.

cross-sectional surface is irradiated with chopped (argon-ion) laser heating beam at normal incidence, and probed with a second (helium-neon) laser probe beam at grazing incidence. The deflection of the probe beam is highly sensitive to the local temperature field, and therefore to crack-like defects,^{6,9} in the immediate specimen subsurface. In the setup depicted in Fig. 1, both heating and probe laser beams are aligned with their planes of incidence normal to the section surface in the contact damage region. The heating and probe spots on the irradiated surface are close but separate, with their spot centers aligned along the vertical plasma spray direction. We monitor the “transverse” (in-plane) component of the deflection,⁵ which is sensitive to the heat flux parallel to the irradiated surface plane.¹⁰ This specific heating/probe beam alignment and transverse mode configuration essentially measures the diffusivity through the thickness of the coating. It is this through-thickness diffusivity that is most pertinent to thermal barrier applications. The probe beam deflection is recorded and digitized, and the specimen rastered over a selected area consisting of an array of $l \times n$ pixels, with the heating and probe beam spatially fixed, to obtain a thermal image of the defect distribution.⁶ The thermal waves sample defects down to a “diffusion depth,”⁵ indicated in Fig. 1 by the bands of graded shading beneath the irradiated cross section.

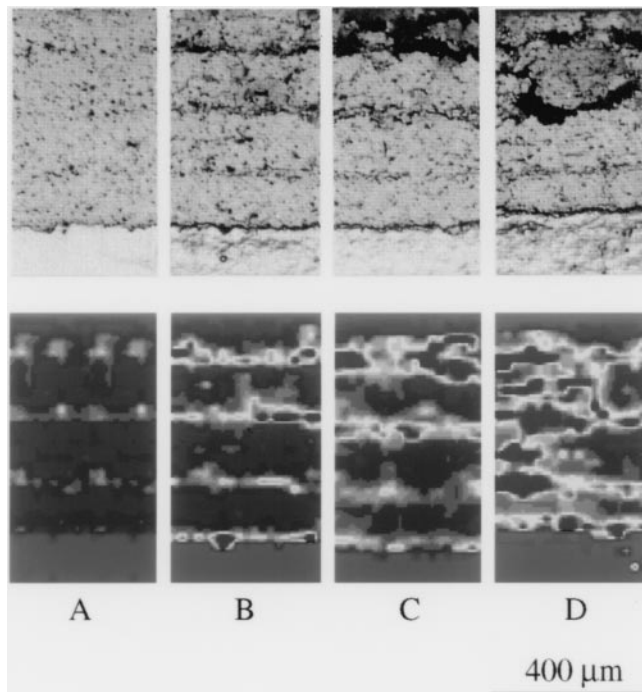


FIG. 4. Optical micrographs (top) and thermal wave images (bottom) of damage areas in alumina coating immediately below contact surface, for number of cycles (A) 0, (B) 1, (C) 10^2 , and (D) 10^5 , at fixed load 500 N.

Figure 2 compares optical and thermal images of contact damage produced in an alumina coating for single cycle loading to a peak 1000 N. In the optical micrograph, Fig. 2(a), fracture damage is evident, preferentially along the defective intralayers and at the coating/substrate interface, together with general yield in both the coating and substrate.⁸ The broad features in this fracture damage pattern are clearly reproduced in the thermal wave image, Fig. 2(b). Signal deflection magnitudes are indicated on the color bar, corresponding to increasing temperature from left to right. (Note that the thermal wave contrast is low in the substrate, owing to high diffusivity in metals relative to ceramics.) The image reveals “hot spots” at the laminar cracks in the coatings, where the laser-generated downward heat flow is abruptly interrupted. Signal deflection profiles along selected columns through the thickness, Fig. 2(c), highlight this local heating effect.

These deflection profiles foreshadow the prospect of quantitative analyses. Taking the digitized probe beam deflection data from the thermal images, an effective through-thickness thermal diffusivity α can be evaluated over any selected window of image area. First, a local value $\alpha_{i,k}$ can be computed for any pixel (i, k) in Fig. 1, using an appropriate deconvolution algorithm.^{6,11} The quantity $\alpha_{i,k}$ is inversely proportional to the “thermal resistance” of the material contained within (i, k) . Then

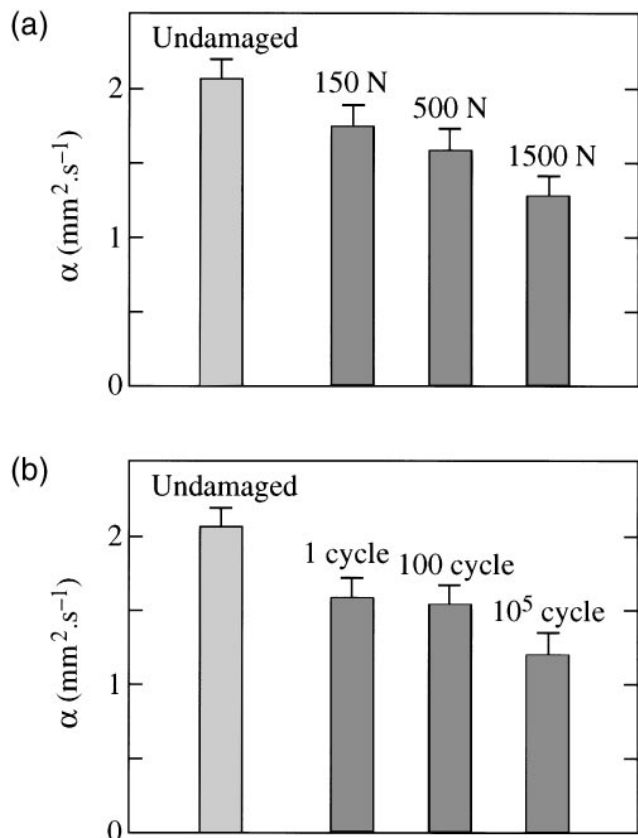


FIG. 5. Plot of effective through-thickness coating diffusivity, as a function of (a) load (single cycle) and (b) number of cycles (fixed load 500 N). Error bars are standard deviations over the α_i summation in Eq. (1).

α can be determined by regarding the (i, k) array as a thermal resistor network, with series connection over all n pixels within the i th column and parallel connection over all l such columns within the selected image area. In terms of diffusivity, we obtain the following equivalent summations:

$$\alpha_i = n / \sum_{k=1}^n (1/\alpha_{i,k}), \quad \alpha = (1/l) \sum_{i=1}^l \alpha_i \quad (1)$$

Thus in Fig. 2 we evaluate $\alpha_i = 1.2 \text{ mm}^2 \cdot \text{s}^{-1}$ for the profile at center and $\alpha_i = 2.2 \text{ mm}^2 \cdot \text{s}^{-1}$ for the profiles at left and right. In this context, the summation at right in Eq. (1) may be viewed as a formulation for smoothing over the sequence of adjacent profiles within a prescribed window of image area, enabling evaluation of a mean and standard deviation for a given specimen. Recalling that the thermal waves penetrate over a diffusion depth, we see that the resultant α pertains to a thin slice of material bounded by the window of irradiated cross section.

To demonstrate how thermal waves may be used to monitor thermal property change from damage accumulation, we show segments of optical and thermal images of subsurface contact regions, with each sequence from a separate specimen: in Fig. 3, as a function of load for a single load cycle; and in Fig. 4, as a function of number of cycles at fixed peak load. The progressive evolution of damage is evident in each case. Corresponding variations in effective diffusivities α evaluated from Eq. 1 over these segments of damage area are plotted in Fig. 5. We see that α diminishes steadily with both increasing load [Fig. 5(a)] and number of cycles [Fig. 5(b)], as might be anticipated. Hence the thermal protection offered to the substrate by the coating actually improves with damage accumulation, up to the point of failure.

The results show the utility of thermal wave techniques, in combination with Hertzian testing, for monitoring the effect of damage evolution on thermal integrity through the lifetime of prospective coating systems to failure. These techniques are amenable to both qualitative and quantitative analysis; and, moreover, provide point-by-point variations, as well as net effective values. Potential uses for evaluating evolving thermal properties in material systems with altogether different defect contents, e.g., from thermal cycling or from processing variation, may be envisioned.

ACKNOWLEDGMENTS

Thanks are due to C.C. Berndt and G. Bancke for supplying the coatings. This work was supported by the U.S. Air Force Office of Scientific Research and the Ministerio de Educación y Ciencia (DGICYT), Spain.

REFERENCES

1. H. Herman, *Sci. Am.* **256**, 113–188 (1988).
2. H. Herman, *Mater. Res. Soc. Bull.* **13**, 60–67 (1988).
3. H. Herman, C. C. Berndt, and H. Wang, in *Ceramic Films and Coatings*, edited by J.B. Wachtman and R.A. Haber (Noyes Publications, Park Ridge, NJ, 1991), pp. 131–188.
4. L. Pawlowski, *The Science and Engineering of Thermal Spray Coatings* (John Wiley, New York, 1995).
5. T. R. Anthony, W. F. Banholzer, J. F. Fleischer, L. Wei, P. K. Kuo, R. L. Thomas, and R. W. Pryor, *Phys. Rev. B* **42**, 1104–1111 (1990).
6. L. Wei and B. R. Lawn, *J. Mater. Res.* **11**, 939 (1996).
7. A. Pajares, L. Wei, B. R. Lawn, N. P. Padture, and C. C. Berndt, *Mater. Sci. Eng.* **A208**, 158–165 (1996).
8. A. Pajares, L. Wei, B. R. Lawn, and C. C. Berndt, *J. Am. Ceram. Soc.* (in press).
9. H. H. K. Xu, L. Wei, N. P. Padture, B. R. Lawn, and R. L. Yeckley, *J. Mater. Sci.* **30**, 869–878 (1995).
10. K. R. Grice, L. J. Inglehart, L. D. Favro, P. K. Kuo, and R. L. Thomas, *J. Appl. Phys.* **54**, 6245–6255 (1983).
11. L. Wei and G. S. White, *J. Mater. Res.* (submitted).